ECS Transactions, 85 (13) 1309-1320 (2018)
10.1149/08513.1309ecst ©The Electrochemical Society

# Nanoporous Membranes by Self-Assembly of "Hairy" Nanoparticles

Yulia Eygeris, Emily White, Amir Khabibullin, Ilya Zharov

Departments of Chemistry and Materials Science and Engineering, University of Utah, Salt Lake City, Utah 84112, and Alexander Butlerov Chemistry Institute, Kazan Federal University, 18 Kremlyovskaya Street, Kazan 420008, Russian Federation

We developed a novel approach to the preparation of nanoporous membranes by the assembly of polymer brush-modified colloidal nanoparticles. Membranes made of uncharged HNPs carrying PHEMA brushes were stable in water, disassembled in organic solvents and could withstand multiple cycles of assembly-disassembly. Their filtration cut-off could be controlled by varying the silica sphere diameter and depends on the polymer brush structure. These membranes can also be recycled and washed from contaminants. Charged HNP membranes containing PSPM-r-PEEMA brushes can be prepared through layered deposition of bare silica and hairy particles. The flux through these membranes responds to the changes in electrolyte concentration. The salt rejection by these membranes is in the moderate to high range (65-80%) and depends on the composition of the polymer brushes and salt concentration.

## Introduction

Membranes are a favored technology for water and wastewater treatment due to no operation prerequisites, with pressure driven separations across membranes being the most widely used water treatment technology.(1) Nanoporous membranes are used to separate suspended solids, viruses, heavy metals, and multi- and mono-valent ions from water. These membranes can be generally classified as ultrafiltration (pore size less than 100 nm) or nanofiltration (less than 10 nm). Such membranes are used in many processes including water treatment, chemical and food production,(2) biosensing,(3,4) drug delivery,(5) catalysis(6,7) and optics.(8) Many of these applications require control over the pore size, a narrow pore size distribution, functional membrane surface, chemical and thermal stability and simple and economical preparation processes.(9,10)

Most commercial nanofiltration membranes are created from polymeric materials because of their ease of production by methods such as phase inversion and interfacial polymerization.(11–15) Polymeric membranes, however, don't have well defined or uniform pores, suffer from inferior stability and their surfaces are difficult to post-functionalize.(12,16) In search of alternative, researchers have turned to inorganic materials such as ceramics,(17,18) gold nanoparticles,(19) silica,(20,21) alumina,(22,23) zeolites,(24,25) and carbon nanotubes.(26,27) These can often be post-functionalized to create a membrane with uniform pores and introduce charge to reduce fouling; however, they have their own set of problems including poor mechanical stability and difficulty achieving a wide range of pore sizes.(28) Regardless of the material, these nanoporous membranes are formed via irreversible covalent bonds and often suffer from pore

blocking and surface fouling during operation. In contrast, membranes formed by non-covalent reversible assembly of molecular or nanoscale building blocks may provide a useful alternative in terms of fabrication, processing, cleaning and reusing and potentially improve membrane lifetime.(29–32) Reversible membranes, formed by non-covalent bonds, would not need to be physically or chemically cleaned; instead, the membrane would only need to be disassembled and then reformed.

Self-assembly of colloidal particles into nanoporous membranes would allow combining the advantages of reversibility with pore size tune-ability, easy functionalization, cheap manufacturing, reusability and attractive material properties such as flexibility. For example, self-assembled gold nanoparticle membranes showed promising nanofiltration characteristics,(33,34) but the small size of the gold nanoparticles and their high cost limit scaling up and achieving a broader pore size range of such membranes.

In the past, we prepared selective and responsive self-assembled supported colloidal films,(34) and covalently-bound free-standing colloidal membranes(35) using silica nanospheres. Colloidal crystals of non-porous silica form in a face-centered cubic (*fcc*) closed-packed lattice, with three-dimensional and interconnected pore network produced by void space between the spheres,(34) with the pore size easily controlled by changing the size of the spheres.(21) They possess size-selectivity tunable by changing the silica particle size(36) and are capable of charge-(35) and enantioselective(37) transport after the suitable silica surface modification. However, the mechanical properties of these membranes and their preparation methods are not ideal.

Here, we describe the preparation of nanoporous membranes via the self-assembly of silica nanospheres modified with polymer brushes, or "hairy" nanoparticles (HNPs). We prepared two different types of HNPs: 1) uncharged, carrying poly(2-hydroxyethyl methacrylate) (PHEMA) brushes; and 2) "*charged*" brushes containing poly(3-sulfopropylmethacrylate) (PSPM). Flux measurements and size cut-off experiments were performed and the collected data was used to estimate the membrane pore size. Charged membranes capable of charge rejection were used to test salt rejection. Presented membranes were found to be capable of both size and charge separation.

## Materials and methods

### Materials

Ethyl 2-bromoisobutyrate, 3-aminopropyltriethoxysilane (APTES), triethylamine, 2-bromoisobutyryl bromide, 3-sulfopropyl methacrylate potassium salt (SPM), 2,2'-bipyridine, 2-ethoxyethyl methacrylate (EEMA), 2-hydroxyethyl methacrylate) (HEMA), copper (I) chloride and monodisperse dextrans of various molecular weights were purchased from Sigma Aldrich. 4-dimethylaminopyridine (DMAP) and tethraethoxysilane (TEOS) were purchased from Alfa Aesar. Dichloromethane (DCM), methanol, ammonia hydroxide solution, sodium chloride, sodium sulfate decahydrate and sodium citrate dihydrate were purchased from Fischer Chemicals. Copper (II) chloride dihydrate was purchased from Acros. Gold nanoparticles were purchased from BBI Solutions and polystyrene spheres were purchased from Polysciences, Inc.

## Methods

Characterization**.** Scanning electron microscopy (Hitachi S3000-N) and transmission electron microscopy (JEOL JEM1400-Plus) were employed to perform the imaging of the materials. Thermogravimetric analysis of polymer-modified particles was conducted using TGA 2950 Thermogravimetric Analyzer (TA Instruments). Branson 1510 sonicator was used for all sonications. UV/Vis measurements were performed using an Ocean Optics USB4000 instrument.

Preparation of silica particles. Silica nanoparticles (SNPs) were prepared using Stober method.(38) Diameter of silica particles is found to be 267±25 nm, 280±30 nm, 390±20 nm and 460±50 nm. Size of nanoparticles was determined by dynamic light scattering (DLS) and confirmed by transmission electron microscopy (TEM).

Grafting of polymerization initiation sites**.** ATRP sites prepared through previously described procedures in two steps(39). On the first step, primary amines were grafted on surface to facilitate addition of initiator sites as follows: suspension of ~2 g of Stober silica particles in 15 mL of dry acetonitrile was purged with nitrogen gas for 15 mins, then 0.2 mL of APTES were injected into the mixture. Reaction mixture was stirred for 24 hours. Aminated particles were collected by centrifugation, washed at least three times with acetonitrile and dried. On the second step, polymerization initiator sites were grafted as follows: to suspension of ~1 g of aminated silica particles in 50 mL anhydrous DCM added 40 mg (0.3 mmol) DMAP, purged with nitrogen gas for 15 mins, then injected 2.09 mL (15 mmol) triethylamine and 1.61 mL (13 mmol) 2-bromoisobutyryl bromide. Reaction was left stirred under room temperature for 24 hours. Resulted particles were collected by centrifugation, washed at least three times with DCM and dried. Successful surface modification on each step was confirmed using thermogravimetric analysis (TGA).

Polymerization of PHEMA. Polymer brushes were grafted through surface-initiated atom-transfer radical polymerization (SI-ATRP).(40) The grafting of PHEMA brushes onto the initiator-modified silica spheres (1 g) was carried out in degassed methanol containing PMDETA, $CuBr_2$, CuBr as well as HEMA (5.7 mmol) at 70 °C for 12 h under the nitrogen atmosphere. The resulting modified particles were washed with methanol and water and dried. Polymer length was estimated using TGA weight loss assuming grafting density of 0.5 brushes/$nm^2$.(41)

Copolymerization of PSPM-r-PEEMA. Grafting of PSPM-r-PEEMA brushes onto the initiator-modified silica spheres (1 g) was carried in degassed methanol/water mixture (2:1 ratio by weight) containing 16 mg (0.1 mmol) $CuCl_2 \cdot 2H_2O$, (250 mg) 1.6 mmol 2,2'-bipyridine and 0.3 mmol CuCl as well as mixture of EEMA and SPM (20 mmol total) at room temperature under the nitrogen atmosphere for up to 6 hours. The polymerization reaction was quenched by exposing the reaction mixture to air and addition of water, washed twice by MeOH and $H_2O$ and left stirring overnight in 1 M HCl. Then, particles were washed twice with $H_2O$, once with MeOH and dried. Desired ratio of monomers was controlled by ratio of introduced monomers as their polymerization rates are similar.(42) Degree of polymerization was calculated using TGA assuming polymer grafting density of 0.2 brushes/$nm^2$.(43)

Membrane formation. 10 mL dead-end filtration cells (Sterlitech Corporation and Millipore Amicron) were used to form the membranes and study flux and solute rejection. A membrane layer was prepared through pressure-driven deposition of colloidal suspension of silica nanoparticles in 10 mL 20% EtOH/$H_2O$ on a macroporous support

(either nylon or regenerated cellulose, nominal pore size 0.2 μm). Pressure was controlled by flow of gas (air) and was set equal to 1 atm unless specified otherwise.

Performance tests. Millipore water with nominal resistivity of 18 MΩ•cm was used in preparation of all solutions and water flow experiments. Aqueous solutions of NaCl, $Na_2SO_4$ and $Na_3C_6H_5O_7$ were used in order to evaluate charge rejection. 5 mL of each solution were driven through the membrane and permeate salt concentration was monitored over time using a conductivity meter (HM Digital Inc., Culver City, CA). Salt rejection was determined as follows:

$$R = (1 - C_p/C_f) \times 100\% \quad [1]$$

where $C_p$ and $C_f$ – concentrations in permeate and feed, respectively. Pore size cutoff was determined using 0.5 g/L solutions of dextrans with different molecular weights (25, 80, 270 and 670 kDa), 0.2% by weight polystyrene sphere suspension (25, 39 and 54 nm), G5 PAMAM dendrimer, and 20 and 40 nm Au particles in water. 5 mL of solution was driven through the membrane under 1 atm applied pressure and amount of permeate was determined spectrophotometrically at wavelength of 492 nm for dextrans using phenol-sulfuric acid method(44), at 240 nm for polystyrene spheres and at 520 nm for gold nanoparticles. The filtrates were analyzed using DLS and UV-Vis spectroscopy. Reported values for dextran and salt rejection are for the first milliliter of permeate as rejection declines overtime due to concentration polarization across membrane. Membranes were washed with solvent between the runs.

Diffusion through the membranes. Diffusion experiments through the colloidal membranes were performed by sealing a piece of a membrane between Teflon rings and placing it between two 1 cm quartz cuvettes. The feed cell contained 4 mL of the permeate in water, while the receiving cell contained 4 mL of water. The molecular flux was monitored by recording the UV-Vis absorbance at 250 nm for PS beads and 200 nm for Au nanoparticles in the receiving cell for at least 12 h. Prior to using a membrane in a new experiment, is was immersed in ethanol or water for at least 24 h and the solvent was replaced occasionally to ensure the removal of any previous probe molecule or particles from the membranes.

Mechanical testing of the membranes. The flexural strength of the free-standing uncharged membranes was estimated using the four-point bending test, as described elsewhere.(21) Rectangular membrane samples were cut using a carbon dioxide laser. The membrane sample was placed on two metal rods of the support span and covered with the loading span that made contact with the sample using two metal rods. A load was applied and increased until the membrane sample fractured, and the rupture force was used to calculate the flexural strength using the following equation:

$$\sigma = Fl/bd^2 \quad [2]$$

where $\sigma$ is flexural strength (Pa), $F$ is rupture force (N), $L$ is support length (m), $b$ is sample width (m) and $d$ is sample thickness (m).(21)

## Results and discussion

Uncharged membranes

Preparation of free-standing membranes and their mechanical properties. We discovered that free-standing nanoporous membranes can be prepared by the assembly of "hairy" silica nanoparticles carrying poly(2-hydroxyethyl methacrylate), PHEMA, brushes (synthesis shown in Figure 1) from ethanol colloidal solutions. The length of PHEMA brushes on 330 nm silica spheres was ~15 nm (determined by DLS) with the average molecular weight of ~6000 g/mol (approx. 48 HEMA monomers per brush), as determined by thermogravimetric analysis (TGA) with 0.5 PHEMA chains per $nm^2$.(41) After ethanol evaporation, a solid material formed as smooth and evenly thick flat pieces of ~2 $cm^2$ area and thickness varying from 0.4 to 0.7 mm depending on the concentration of the "hairy" spheres in colloidal solution. SEM images of the membranes (Figure 2A) showed closely packed yet disordered silica spheres. The SEM images of the membrane cross-section (Figure 2B-C) demonstrate that the "hairy" particles form a continuous assembly without mechanical defects and with a smooth surface.

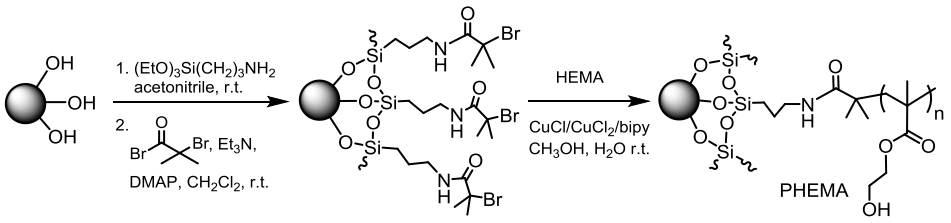


Figure 1. Preparation of PHEMA brushes on the surface of silica spheres

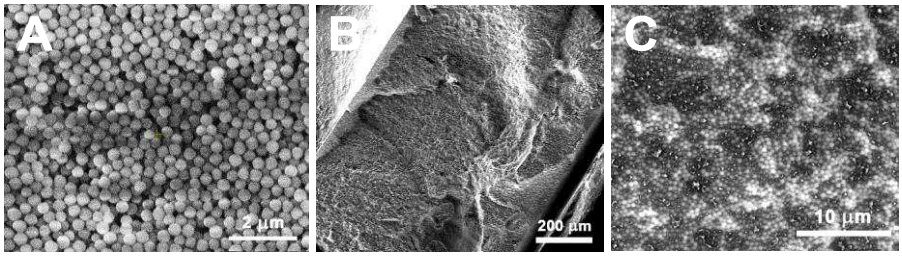


Figure 2. Representative SEM images of the top (A) and cross-section (B-C) view of uncharged membrane

The flexural strength of the membranes was found to be 0.5±0.1 MPa using the 4-point bending test. This flexural strength was significantly smaller than that of sintered silica colloidal membranes (49±9 MPa),(35) which is expected as self-assembled membranes form via non-covalent interactions between the "hairy" particles while sintered membranes form by creation of strong Si-O-Si covalent bonds. Despite the low flexural strength, the uncharged membranes can be handled, sonicated, sandwiched between plastic or metal rings, and even dropped from 1 m height without breaking or cracking. Moreover, uncharged membranes were stable in water, but softened in ethanol and acetonitrile within ~30 minutes. Sonication of the membranes lead to complete dispersion after only 15 minutes. This behavior of uncharged membranes can be explained by changing the polymer-solvent interactions depending on the solvent quality. PHEMA brushes swell significantly in organic solvents such as ethanol and methanol, which causes the membranes to disassemble, while water solvates PHEMA to a lesser extent.(45)

Transport through uncharged membranes. Water flux through a membrane is its important characteristic, as it provides an insight into the membrane structure and integrity and greatly affects separation quality and speed. In order to characterize the water flux, we prepared uncharged membranes supported on regenerated cellulose disk. The flux of water through the 1.3 mm thick membrane made of 460 nm PHEMA-modified silica spheres deposited on regenerated cellulose support with 0.2 μm pores under 0.35 bar pressure was 18 $L \cdot m^{-2} \cdot hr^{-1}$ (51 $L \cdot m^{-2} \cdot bar^{-1} \cdot hr^{-1}$). Applying a higher pressure resulted in a higher flux. The average water flux through the uncharged membranes under 1.45 bar was 103 $L \cdot m^{-2} \cdot hr^{-1}$ (71 $L \cdot m^{-2} \cdot bar^{-1} \cdot hr^{-1}$). All of measured flux values exceed the flux of commercially available ultrafiltration and nanofiltration membranes (1 – 13 $L \cdot m^{-2} \cdot bar^{-1} \cdot hr^{-1}$).(46) Thus, uncharged membranes can be potentially applied in ultrafiltration and water purification systems.

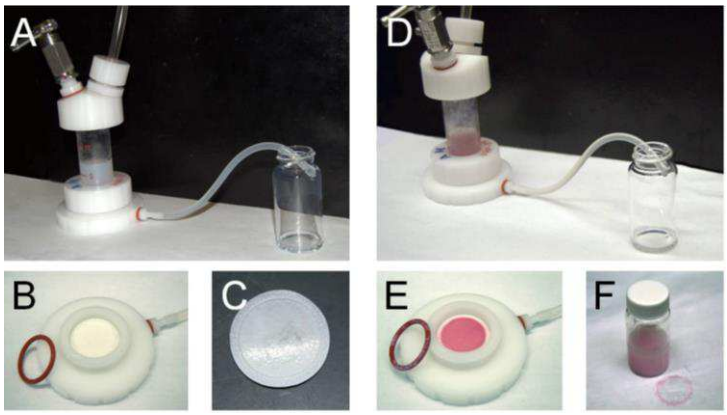


Figure 3. Preparation of supported "neutral" membrane and isolation of Au nanoparticles. (A) Formation of "neutral" membrane on cellulose support inside stirred cell. (B) Disassembled stirred cell with "neutral" membrane on support. (C) Supported membrane. (D) Ultrafiltration of 20 nm Au nanoparticles through "neutral" membrane made of 280 nm "hairy" silica spheres. (E) Disassembled stirred cell with Au nanoparticles trapped inside the "neutral" membrane. (F) Dispersed "neutral" membrane with Au nanoparticles in solution.

Solute transport through a membrane can generally be explained in terms of steric hindrance and electrostatic models.(47) In the case of HNP membranes with uncharged brushes, steric hindrance is the only mechanism and rejection of solutes is defined by the relationship between pore and solute sizes. If solute radius $r_{solute} \geq r_{pore}$, solute will be retained by the membrane.(48)

We tested the diffusion of different solutes, G5 PAMAM dendrimer (diameter 6 nm) and 20 and 40 nm gold nanoparticles, in water in order to determine the pore size cut-off of the uncharged membranes. A free-standing membrane made of 330 nm silica spheres had the pore size cut-off of 20 nm, as determined from the fact that G5 PAMAM dendrimer permeated the membrane while and 20 nm gold nanoparticles were retained by the membrane. To demonstrate the tunability of the pore size in the uncharged membranes, we prepared membranes using "hairy" uncharged silica spheres of two different diameters (280 and 460 nm) on nylon supports with 0.2 μm pore size (Figure 3A-C). We found that the membrane made of 280 nm HNPs possessed the pore size cut-off of 20 nm. The noticeable retention of 20 nm gold particles is illustrated in Figure 3D,E. The membrane made of 460 nm HNPs possessed a larger cut-off of 40 nm. These cut-offs are smaller than those calculated for the close-packed silica colloidal crystals made of 280 and 460 nm spheres (44 and 70 nm, respectively), which we attribute to the presence of PHEMA brushes. These results demonstrate that uncharged HNP membranes

are capable of size-selective ultrafiltration and that their pore size can be easily tuned by changing the silica spheres size, and potentially polymer brush length.

The uncharged membranes with trapped gold nanoparticles could be dispersed in ethanol, forming a colloidal solution containing "hairy" silica spheres and gold nanoparticles (Figure 3F). After the sonication, the heavier silica particles can be precipitated by centrifugation while the small gold nanoparticles remain in solution and can be isolated. The collected silica spheres can be re-dispersed in ethanol and deposited to form the regenerated ultrafiltration membrane without loss of performance.

Negatively charged membranes

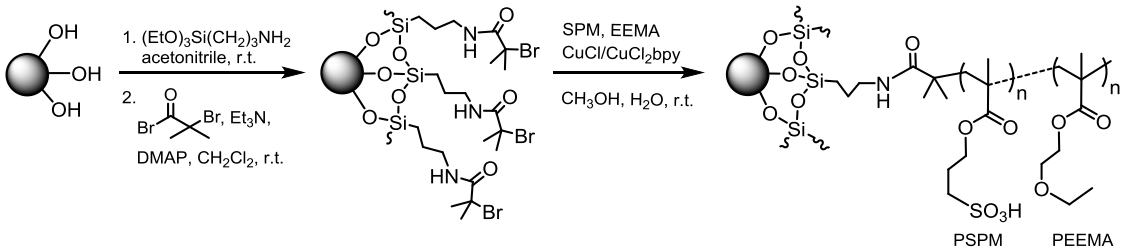


Figure 4. Preparation of PSMP/PEEMA brushes

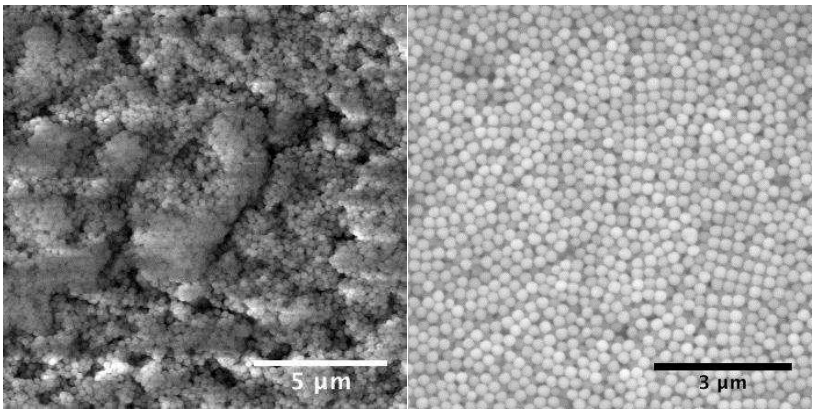


Figure 5. Effect of different degrees of sulfonation on particle packing: left - 10%, right - 17% sulfonation

Membrane preparation. In order to assemble the negatively charged HNP membranes we used "hairy" nanoparticles carrying polymer brushes containing 3-sulfopropyl-methacrylate (SPM) and 2-ethoxyethyl methacrylate (EEMA) prepared as shown in Figure 4. The degree of sulfonation (percent of charged monomers in a polymer chain) could be controlled by changing the monomer ratio as polymerization rates of SPM and EEMA monomers are similar.(42) EEMA monomer was chosen in order to offset the hydrophilicity of the SPM monomer and improve the overall membrane stability. The properties of the membranes assembled using charged HNP depended on the composition of the polymer brushes. When the amount of SPM in the polymer was below 17%, the resulting membranes possessed irregular structures as seen in their SEM images (Figure 5, left). However, above 17% SPM the particles formed uniform porous films with relatively ordered arrangement of the nanoparticles (Figure 5, right). Such membranes could be formed with HNPs containing up to 35% SPM in the polymer brushes. Above this ratio the resulting membranes disintegrated in water. In addition, we found that in order to obtain membranes with reproducible flux a layer of bare silica has to be

deposited on the surface of the nylon support before the PSPM-r-PEEMA HNP membrane formation. For further performance tests, we selected charged "hairy" particles containing polymer brushes ranging in length from 100 to 500 monomer units (17 to 95 kDa) (estimated using thermogravimetric analysis (TGA) data for grafting density of 0.2 brushes/nm$^2$(43)) and in degree of sulfonation from 17% to 35% on silica spheres of 270 nm in diameter. These particles are coded below as 100-17S and 500-35S, respectively.

Pore size cut-off. First, we attempted testing the permeation of gold nanoparticles ranging from 5 to 40 nm in diameter to determine the pore size in a way similar to that described above for uncharged membranes. However, we discovered that gold particles fully adhere to the HNP surface regardless of their concentration. While adsorption of gold particles on bare silica is a known phenomenon widely utilized in the field of plasmonic materials,(49) we did not anticipate gold particle adsorption for PSPM-r-PEEMA HNP membrane, especially considering our previous successful experiments using gold particles. We believe that this is the result of gold particles being coordinated by the charged polymer brushes. As a result, we switched to the use of neutral solutes such as polystyrene beads(50) and dextrans.(51)

After monitoring the permeation of dextrans varying in diameter from 7 nm to 31 nm (based on $M_w$ 25 to 670 kDa and using $d$(Å) = 0.66M$_w^{0.46}$ to calculate the diameter(52)) through the charged membranes, we observed only minor dextran rejection ($R_{ave}$ ~ 18%) with no dependence on molecular weight and no change in water flux throughout the experiment. Next, we tested the permeation of polystyrene beads. The PS beads with diameter of 54 nm were completely filtered out by the membrane, therefore, considering the results of the dextrans, the membrane pore size is between 31 to 54 nm.

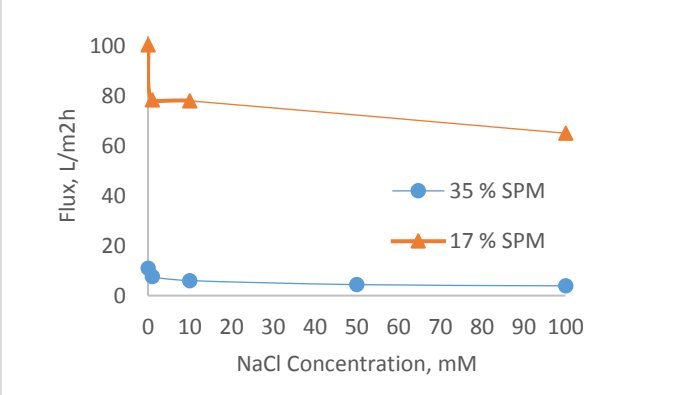


Figure 6. Flux as a function of NaCl concentration

Water flux as a function of ionic strength. Charged polymer brushes are known to undergo conformational changes and consequently change the polymer length in the presence of electrolytes. For example, positively charged poly-4-vinyl(N-methyl-pyridinium) brushes grafted onto a planar surface swell as salt concentration increases and then collapse when the concentration of co-ions in solution is equal to or greater than the concentration of free counter ions in the brush due to electrostatic screening.(53) This results in increasing and decreasing polymer brush height as polymer swells and collapses, respectively. Similar observations have been made for negatively charged poly(sodium styrenesulfonate) brushes on a planar surface.(54) The grafting density of the chains was shown to significantly affect this behavior.(53,55)

The polymer swelling can have a significant effect on the pore size in HNP membranes. To confirm whether the presence of salt solutions has an effect on polymer

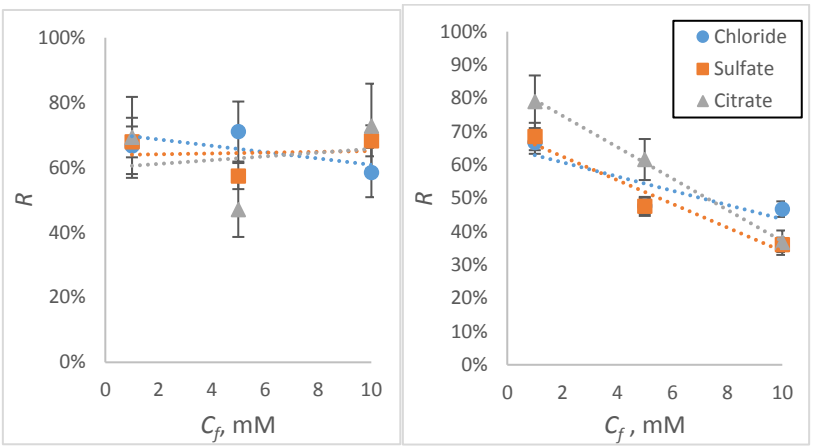


Figure 7. Salt rejection as function of salt feed concentration: left – 100-17%, right - 500-35%; dashed lines are the guides for the eye. The first number in sample name indicates degree of polymerization and the second stands for degree of sulfonation

brushes in charged "hairy" particle membranes, we measured the flux of NaCl solutions of various concentrations through these membranes. We observed a significant decrease in flux as the salt concentration increased (Figure 6). The flux changed 1.5-fold for 100-17S membranes (from 100 to 65 $L \cdot m^{-2} \cdot bar^{-1} \cdot hr^{-1}$) and 3-fold for 500-35S membranes (from 12 to 4 $L \cdot m^{-2} \cdot bar^{-1} \cdot hr^{-1}$), which likely results from a partial blockage of the pores due to swelling of the polymer brushes.

Salt rejection. As mentioned above, membrane transport through nanopores can be described by electrostatic and sieving mechanisms.(56,57) Retention of uncharged solutes is determined by the relationship between the pore and solute size, while charged solutes are transported based on electrostatic interactions with the charged membrane.(58,59) Rejection of charged species in charged nanopores can be described using the Donnan model(60) as follows:

$$R = (1 - C_p/C_f) \times 100\% = (1 - (|z_i|C_f/(|z_i|C_p + X))^{|z_i/z_j|}) \times 100\% \quad [4]$$

where $R$ – rejection of electrolyte solution, $C_f$ and $C_p$ - concentration of co-ions in the feed and permeate solutions, respectively, $X$ - membrane charge density, $z$ - ion valence, subscripts $i$ and $j$ refer to co- and counter- ions to membrane charge. Thus, co- and counter- ion charges play substantial role in determining the membrane rejection if the Donnan model is the applicable description of the salt rejection mechanism. However, the Donnan model is limited by the assumption that charge rejection occurs solely due to the interaction between the charges of the free ions and the membrane surface without experiencing steric hindrance due to pore size or tortuosity.(47,61)

**Table 1**. Water flux and salt rejection for negatively charged HNP membranes.

| Sample (DP-%SPM) | $J$, $L/m^2bar \cdot hr$ | Salt rejection $R$, % | | | |
|---|---|---|---|---|---|
| | | $C_f$, mM | NaCl | $Na_2SO_4$ | $Na_3C_6H_5O_7$ |
| 100-17% | 103±4 | 1 | 67±13 | 68±5 | 69±18 |
| | | 5 | 71±17 | 57±3 | 47±6 |
| | | 10 | 58±6 | 68±7 | 73±8 |
| 500-35% | 11±1 | 1 | 67±18 | 69±6 | 79±14 |
| | | 5 | 48±5 | 48±5 | 62±5 |
| | | 10 | 47±1 | 36±6 | 37±4 |

To test whether the charged HNP membranes follow the Donnan exclusion model we measured the permeation of strong electrolytes (sodium chloride, sulfate and citrate) through the HNPs membranes with two different polymer brush compositions. The results are shown in Table 1 and illustrated in Figure 7. All membranes had negative charge due to the abundance of sulfonic groups in the polymer brushes. Therefore, according to the Donnan model, the salt rejection should increase with increasing co-ion charge such as $R$ (NaCl) < $R$ ($Na_2SO_4$) < $R$ ($Na_3C_6H_5O_7$) and decrease with increasing concentration due to the screening of the membrane charges with an abundance of counter-ions. It can be also anticipated that the salt rejection will increase with increasing number of sulfonic groups in the polymer, which increases the charge density of the membrane.

We have observed two types of salt rejection behavior: (1) 100-17S membranes showed a relatively high salt rejection (~65%) and no concentration or ion valence effect; (2) 500-35S membranes showed higher salt rejection (~80%) decreasing with concentration, with citrate generally having higher rejection than that of chloride and sulfate. Thus, only the 500-35S membranes displayed the behavior expected based on the Donnan model. Considering the aforementioned observation of polymer brush swelling, we believe that the behavior of 100-17S membranes is due to a combination of conformational and electrostatic effects. In the case of 100-17S membranes, polymer brushes are short but extend into the pores with increasing salt concentration, therefore increasing the charge density inside the pores. This swelling behavior compensates for the charge screening due to the increasing salt concentration, therefore keeping the overall rejection constant and independent of the concentration. On the other hand, longer charged polymer brushes such as those of 500-35S HNPs may undergo less swelling in response to the increase in salt concentration, so the screening of the membrane surface charge prevails and reduces the salt rejection. Attempts to fit the membrane charge density parameter $X$ using rejection values in terms of the Donnan model were unsuccessful for both of the membranes, leading us to conclude that conformational effects play a role in the observed salt rejection behavior and that observed differences in salt rejection are the result of competing conformational and electrostatic effects.

## Conclusion

We developed a novel approach to the preparation of nanoporous membranes by the assembly of polymer brush-modified colloidal nanoparticles. Membranes made of uncharged HNPs carrying PHEMA brushes were stable in water, disassembled in organic solvents and could withstand multiple cycles of assembly-disassembly. Their filtration cut-off could be controlled by varying the silica sphere diameter and depends on the polymer brush structure. These membranes can also be recycled and washed from contaminants. Charged HNP membranes containing PSPM-r-PEEMA brushes can be prepared through layered deposition of bare silica and hairy particles. The water flux through these membranes responds to the changes in electrolyte concentration. The salt rejection by these membranes is in the moderate to high range (65-80%) and depends on the composition of the polymer brushes and salt concentration. The ability to control the pore size and charge, high flux, durability, flexibility, time- and cost-efficiency, and the ability to recover the retentate and clean the membranes by disassembly makes HNP membranes a promising material for ultrafiltration and size- and charge-selective separations.

## Acknowledgments

This work has been supported by the National Science Foundation (grant no. CHE-1710052) and the Russian Science Foundation (grant no. 18-13-00149).

## References

1. M. M. Pendergast and E. M. V. Hoek, *Energy Environ. Sci.*, **4**, 1946–1971 (2011).
2. K. Scott, *Handbook of Industrial Membranes*, 1st ed., Elsevier Science Publishers LTD, Oxford, (1995).
3. J. Deng and C.-S. Toh, *Sensors*, **13**, 7774–7785 (2013).
4. K. Hotta, A. Yamaguchi, and N. Teramae, *J. Phys. Chem. C*, **116**, 23533–23539 (2012).
5. G. Jeon, S. Y. Yang, and J. K. Kim, *J. Mater. Chem.*, **22**, 14814 (2012).
6. L. Wei and K. Kawamoto, *Chem. Eng. Technol.*, **36**, 650–656 (2013).
7. Q. Li, S. Cui, and X. Yan, *J. Solid State Electrochem.*, **16**, 1099–1104 (2012).
8. Q. Zhao et al., *J. Am. Chem. Soc.*, **135**, 5549–5552 (2013).
9. S. P. Adiga, C. Jin, L. A. Curtiss, N. A. Monteiro-Riviere, and R. J. Narayan, *Wiley Interdiscip. Rev. Nanomedicine Nanobiotechnology*, **1**, 568–581 (2009).
10. P. Stroeve and N. Ileri, *Trends Biotechnol.*, **29**, 259–66 (2011).
11. S. P. Nunes and K.-V. Peinemann, Eds., *Membrane Technology in the Chemical Industry*, Wiley-VCH, (2006).
12. S. Jons, P. Ries, and C. J. McDonald, *J. Memb. Sci.*, 79–99 (1999).
13. M. Ulbricht, *Polymer (Guildf)*, **47**, 2217–2262 (2006).
14. K.-V. Peinemann, V. Abetz, and P. F. W. Simon, *Nat. Mater.*, **6**, 992–996 (2007).
15. S. E. Querelle, E. A. Jackson, E. L. Cussler, and M. A. Hillmyer, *ACS Appl. Mater. Interfaces*, **5**, 5044–5050 (2013).
16. H. Siddique et al., *Ind. Eng. Chem. Res.*, **52**, 1109–1121 (2013).
17. K. Peng Lee and D. Mattia, *J. Memb. Sci.*, **435**, 52–61 (2013).
18. Y. Chang, Z. Ling, Y. Liu, X. Hu, and Y. Li, *J. Mater. Chem.*, **22**, 7445 (2012).
19. K. E. Mueggenburg, X.-M. Lin, R. H. Goldsmith, and H. M. Jaeger, *Nat. Mater.*, **6**, 656–660 (2007).
20. S. Onclin, B. J. Ravoo, and D. N. Reinhoudt, *Angew. Chemie - Int. Ed.*, **44**, 6282–6304 (2005).
21. A. Khabibullin and I. Zharov, *ACS Appl. Mater. Interfaces*, **6**, 7712–7718 (2014).
22. C. S. Toh, B. M. Kayes, E. J. Nemanick, and N. S. Lewis, *Nano Lett.*, **4**, 767–770 (2004).
23. A. Yamaguchi et al., *Nat. Mater.*, **3**, 337–341 (2004).
24. S. Kallus et al., *J. Mater. Chem.*, **12**, 3343–3350 (2002).
25. A. S. T. Chiang and K. Chao, *J. Phys. Chem. Solids*, **62**, 1899–1910 (2001).
26. B. J. Hinds et al., *Science (80-. ).*, **303**, 62–65 (2004).
27. S. A. Miller and C. R. Martin, *J. Am. Chem. Soc.*, **126**, 6226–6227 (2004).
28. P. Guo et al., *Small*, **1703493**, 1703493 (2018).
29. E. Krieg, H. Weissman, E. Shirman, E. Shimoni, and B. Rybtchinski, *Nat. Nanotechnol.*, **6**, 141–146 (2011).
30. Y. Lu, T. Suzuki, W. Zhang, J. S. Moore, and B. J. Mariñas, *Chem. Mater.*, **19**, 3194–3204 (2007).

31. S. P. Nunes et al., *ACS Nano*, **5**, 3516–3522 (2011).
32. R. Hilke et al., *ACS Appl. Mater. Interfaces*, **5**, 7001–7006 (2013).
33. J. He et al., *Nano Lett.*, **11**, 2430–2435 (2011).
34. I. Zharov and A. Khabibullin, *Acc. Chem. Res.*, **47**, 440–449 (2014).
35. A. K. Bohaty, J. J. Smith, and I. Zharov, *Langmuir*, **25**, 3096–3101 (2009).
36. P. A. Ignacio-de Leon and I. Zharov, *Chem. Commun.*, **47**, 553–555 (2011).
37. P. A. Ignacio-De Leon et al., *Isr. J. Chem.*, **54**, 767–773 (2014).
38. W. Stöber, A. Fink, and E. Bohn, *J. Colloid Interface Sci.*, **26**, 62–69 (1968).
39. A. Khabibullin, E. Fullwood, P. Kolbay, and I. Zharov, *ACS Appl. Mater. Interfaces*, **6**, 17306–12 (2014).
40. P. McCarthy, N. V. Tsarevsky, L. Bombalski, K. Matyjaszewski, and C. Pohl, *ACS Symp. Ser.*, **944**, 252–268 (2006).
41. J. Choi, H. Dong, K. Matyjaszewski, and M. R. Bockstaller, *J. Am. Chem. Soc.*, **132**, 12537–12539 (2010).
42. A. Khabibullin, S. D. Minteer, and I. Zharov, *J. Mater. Chem. A*, **2**, 12761 (2014).
43. M. Biesalski and J. Rühe, *Macromolecules*, **36**, 1222–1227 (2003).
44. M. Dubois, K. A. Gilles, J. K. Hamilton, P. A. Rebers, and F. Smith, *Anal. Chem.*, **28**, 350–356 (1956).
45. R. Campan, F. Cazaux, and X. Coqueret, *Macromol. Mater. Eng.*, **287**, 924–930 (2002).
46. A. S. Pine, N. Menyuk, and G. Dresselhaus, *Solid State Commun.*, **31**, 187–191 (1979).
47. X.-L. Wang, T. Tsuru, S. Nakao, and S. Kimura, *J. Memb. Sci.*, **103**, 117–133 (1995).
48. J. Schaep, B. Van der Bruggen, C. Vandecasteele, and D. Wilms, in *Chemistry for the Protection of the Environment 3*,, p. 117–125, Springer US, Boston, MA (1998).
49. M. L. Brongersma, *Nat. Mater.*, **2**, 296–297 (2003).
50. M. Faccini et al., *J. Nanomater.*, **2015**, 1–9 (2015).
51. B. Van der Bruggen, J. Schaep, D. Wilms, and C. Vandecasteele, *J. Memb. Sci.*, **156**, 29–41 (1999).
52. K. A. Granath and B. E. Kvist, *J. Chromatogr. A*, **28**, 69–81 (1967).
53. M. Biesalski, D. Johannsmann, and J. Rühe, *J. Chem. Phys.*, **120**, 8807–8814 (2004).
54. T. Wang et al., *Langmuir*, **30**, 12850–12859 (2014).
55. H. Zhang and J. Rühe, *Macromolecules*, **38**, 4855–4860 (2005).
56. W. R. Bowen, a. W. Mohammad, and N. Hilal, *J. Memb. Sci.*, **126**, 91–105 (1997).
57. A. E. Childress and M. Elimelech, *Environ. Sci. Technol.*, **34**, 3710–3716 (2000).
58. J. Schaep, B. Van der Bruggen, C. Vandecasteele, and D. Wilms, *Sep. Purif. Technol.*, **14**, 155–162 (1998).
59. M. R. Teixeira, M. J. Rosa, and M. Nyström, *J. Memb. Sci.*, **265**, 160–166 (2005).
60. F. G. Donnan, *Chem. Rev.*, **1**, 73–90 (1924).
61. X. L. Wang, T. Tsuru, S. I. Nakao, and S. Kimura, *J. Memb. Sci.*, **135**, 19–32 (1997).